SYMBIOSIS

Prophage proteins alter long noncoding RNA and DNA of developing sperm to induce a paternal-effect lethality

Rupinder Kaur[1,2,3]*, Angelina McGarry[1,2], J. Dylan Shropshire[3,4], Brittany A. Leigh[3], Seth R. Bordenstein[1,2,3]*

The extent to which prophage proteins interact with eukaryotic macromolecules is largely unknown. In this work, we show that cytoplasmic incompatibility factor A (CifA) and B (CifB) proteins, encoded by prophage WO of the endosymbiont *Wolbachia*, alter long noncoding RNA (lncRNA) and DNA during *Drosophila* sperm development to establish a paternal-effect embryonic lethality known as cytoplasmic incompatibility (CI). CifA is a ribonuclease (RNase) that depletes a spermatocyte lncRNA important for the histone-to-protamine transition of spermiogenesis. Both CifA and CifB are deoxyribonucleases (DNases) that elevate DNA damage in late spermiogenesis. lncRNA knockdown enhances CI, and mutagenesis links lncRNA depletion and subsequent sperm chromatin integrity changes to embryonic DNA damage and CI. Hence, prophage proteins interact with eukaryotic macromolecules during gametogenesis to create a symbiosis that is fundamental to insect evolution and vector control.

The extent to which bacteriophage proteins in symbiotic bacteria modulate eukaryotic macromolecules has largely been overlooked, except for some virulence proteins and observations of physical interactions within eukaryotic cells (*1*). A prophage-containing bacterial symbiont, *Wolbachia pipientis*, inhabits the reproductive tract of approximately half of all arthropod species worldwide (*2*) and selfishly alters host reproduction to increase the relative number of symbiotic females that transmit the bacteria to the next generation (*3*). Cytoplasmic incompatibility (CI) is the most commonly studied reproductive alteration that impacts arthropod evolution (*4*) and major vector control efforts for population suppression and replacement strategies (*5*–*8*). Specifically, CI results in embryonic death when symbiotic males mate with aposymbiotic females. Nullification of death and thus, rescue of CI, occurs when transmitting females and their eggs harbor the same strain of *Wolbachia* (*9*).

CI is caused by male germline expression of two *cytoplasmic incompatibility factor* genes, *cifA* and *cifB*, encoded by prophage WO in the *w*Mel strain of *Wolbachia* from *Drosophila melanogaster* (*10*, *11*); rescue occurs by expression of *cifA* alone in ovaries (*12*). We recently established that the *w*Mel CifA and CifB proteins invade developing sperm nuclei and alter the abundance of histone and protamine nucleoproteins essential for fertility in *D. melanogaster* (*13*). However, the action of the Cif proteins raises the question of how they incipiently modulate developing sperm macromolecules to impair nucleoprotein composition. In this work, we show that the Cif proteins modify long noncoding RNA (lncRNA) and DNA content of developing sperm early in spermatogenesis to trigger a developmental cascade that results in sperm chromatin integrity changes and induction of CI. Our findings link arthropod reproductive biology and prophage-facilitated bacterial modulation of sperm RNA and DNA macromolecules.

[1]Pennsylvania State University, Departments of Biology and Entomology, University Park, PA 16802, USA. [2]One Health Microbiome Center, Huck Institutes of the Life Sciences, Pennsylvania State University, University Park, PA 16802, USA. [3]Vanderbilt University, Department of Biological Sciences, Nashville, TN 37235, USA. [4]Department of Biological Sciences, Lehigh University, Bethlehem, PA 18015, USA.
*Corresponding author. Email: r.kaur@psu.edu (R.K.); s.bordenstein@psu.edu (S.R.B.)

CifA and CifB are in vitro nucleases

To resolve CifA's molecular function, we used a machine learning tool called CLEAN (*14*). CifA was identified as a site-specific type II restriction endonuclease ($P < 0.001$) whose family of enzymes cleave DNA and strands of RNA-DNA heteroduplexes (*15*). CifB variants are deoxyribonucleases (DNases) with active PDDEXK nuclease domains (*16*, *17*), and sequence homologs across CifB evolution broadly contain these domains (*10*, *11*, *18*). Thus, we investigated prophage protein functions with in vitro enzymatic assays to systematically determine the ribonuclease (RNase) and DNase activity of biochemically uncharacterized Cif proteins from *w*Mel. We generated CifA and CifB proteins by recombinant expression (Fig. 1A) and incubated them with single-stranded (ss) DNA, double-stranded (ds) DNA, and ssRNA oligonucleotide substrates. Purified CifA cleaved ssDNA, dsDNA, and ssRNA substrates (Fig. 1B). Nuclease activity was halted in the presence of the chelating agent ethylenediaminetetraacetic acid (EDTA). Mass spectrometry of the purified proteins revealed small amounts of *Escherichia coli* ribonuclease peptide in purifications of CifA (7 of 1470 total spectral count) and CifB (2 of 3150) (data S1). However, eight-fold-diluted CifA degraded RNA in vitro (fig. S1A), whereas CifB at the same dilution lacked any RNase activity (see below), supporting a causal link between the CLEAN-predicted annotation for CifA and its in vitro RNase activity.

CifB was synthesized without its deubiquitinase (DUB) domain ($CifB_{\Delta D}$) (Fig. 1A and raw data), because full-length CifB is too large to express in recombinant *E. coli* (*19*). $CifB_{\Delta D}$ cleaved ssDNA and dsDNA substrates similarly to the control DNase enzyme, but lacked RNase activity against a ssRNA oligonucleotide substrate (Fig. 1B). EDTA inhibited the DNase function as expected. Enzymatic activity decreased with lower enzyme concentrations and shorter incubation times (fig. S1). Mass spectrometry showed that no copurified *E. coli* DNases were present that might confound the result (data S1). CifB possesses a QxxxY motif within a region of predicted α helices at the C-terminal nuclease domain (fig. S2). This motif is characteristic of RecB-family nucleases with HsdR subunits of *E. coli* that contain a PDDEXK domain (*20*). Mutating Q and Y residues impaired EcoR124I DNA cleavage, possibly by destabilizing the catalytic pocket or modulating the binding efficacy of this domain to the DNA (*21*). The presence of the QxxxY motif in CifB associated with its DNase activity (fig. S2), as the mutant protein with alanine substitutions at the Q and Y residues ($CifB_{QY}$) failed to cleave ss- and dsDNA (Fig. 1, A and B). CifA also possesses a QxxxY motif within a predicted α helix (fig. S2); however, the mutant protein ($CifA_{QY}$) maintained its dsDNA and ssRNA cleaving activity despite its loss of ssDNAase function (Fig. 1B), which indicated that the QxxxY motif may not be functionally essential to the CifA nuclease activity in vitro. These results showed that CifB from *w*Mel *Wolbachia* is a DNase, contrary to previous reports (*11*), and that the QxxxY motif is necessary for its DNase function.

CifA-mediated depletion of lncRNA in spermatocytes strengthens CI

Having validated the respective RNase and DNase properties of CifA and CifB in vitro, we next used transgenic and cytochemical approaches to test the effect of Cifs in vivo against RNA and DNA of developing sperm. In *Drosophila*, several mitotic divisions produce primary spermatocytes (spermatogenesis) before they enter meiosis to form elongating spermatids (spermiogenesis). Genes in primary spermatocytes are actively transcribed for spermiogenesis (*22*). lncRNAs predominantly transcribed

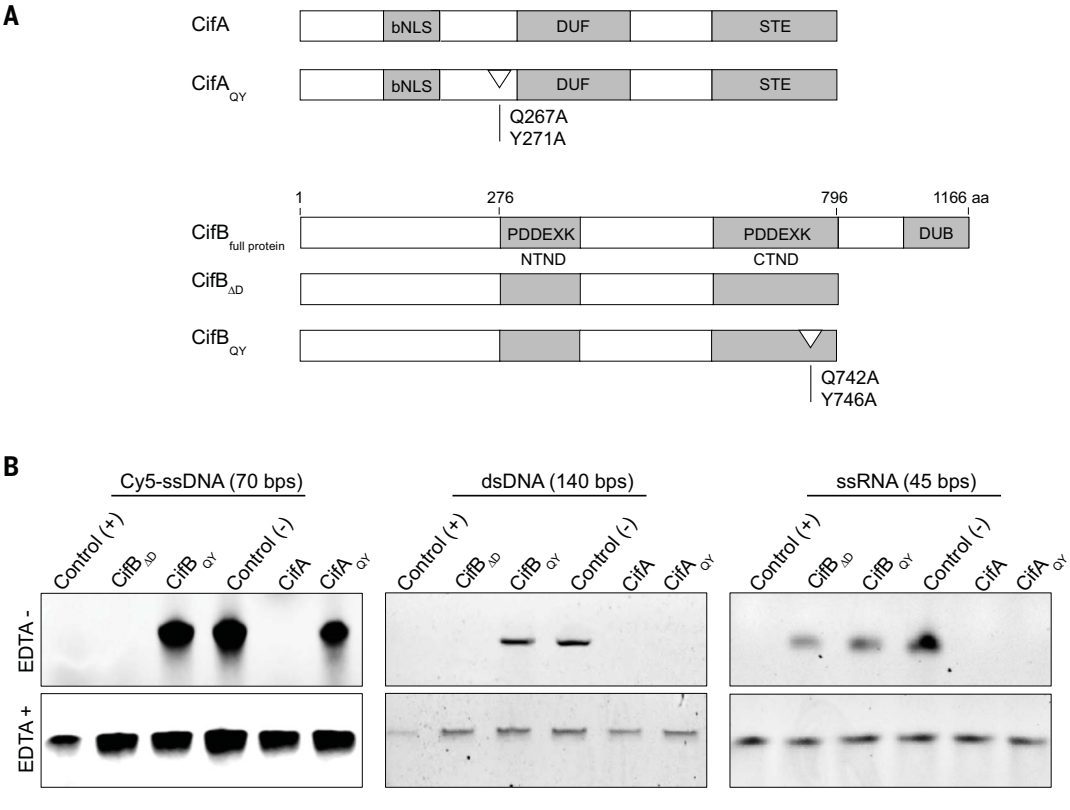

Fig. 1. CifA is an in vitro DNase and RNase, and CifB is a DNase. (**A**) Schematic representation showing the Cif recombinant proteins used in the study. Domain annotations are based on structural homology-based analyses (*18*). The full histidine (His)–tagged CifA protein was generated with ($CifA_{QY}$) and without (CifA) substitutions in the QxxxY motif. Because the full length CifB protein was too large to be recombinantly expressed in *E. coli*, purified His–glutathione *S*-transferase–tagged CifB variants were generated with the amino terminus, N-terminal nuclease domain (NTND), and C-terminal nuclease domain (CTND), refered to $CifB_{\Delta D}$, along with engineered substitutions in the QxxxY motif ($CifB_{QY}$). (**B**) Nuclease activities of the Cif proteins against single-stranded (ss) DNA, double-stranded (ds) DNA, and ssRNA substrates. $CifB_{\Delta D}$ cleaves both ss- and dsDNA but not RNA. QxxxY motif substitutions ablate CifB DNase activity. CifA is both a DNase and RNase. The $CifA_{QY}$ mutant ablates ssDNase activity, whereas dsDNase and ssRNase activities remain intact. Commercial DNase and RNase enzymes were used as positive controls, and no CifA or CifB proteins were added to the reaction mixtures for negative controls. EDTA was added to a 20-fold molar excess over Mg^{2+} to inhibit the reactions. Samples were run in a 10% polyacrylamide–tris-borate EDTA gel. Single-letter abbreviations for the amino acid residues referenced throughout are as follows: Q, Glu; Y, Tyr; A, Ala; G, Gly.

in *Drosophila* testes play a crucial role in chromatin organization during sperm development and male fertility (*23*, *24*). lncRNA derived from AAGAG tandem repeats in heterochromatic regions are highly expressed in primary spermatocytes, and depletion results in a defective histone-to-protamine (H-P) transition during sperm chromatin organization (*25*). We previously showed that *w*Mel and transgenic *cif* expression under a germline-specific driver, nanos-Gal4:VP16 (nos), impairs the H-P transition to induce CI (*13*). Thus, we hypothesized that CifA might degrade AAGAG lncRNA, among others, owing to CifA's RNase activity and alter the H-P transition to establish CI.

We dissected <8-hour-old wild-type (*w*Mel+ and *w*Mel–) and nos-driven transgenic *cif*-expressing fly testes and measured the abundance of the AAGAG lncRNA in primary spermatocytes using fluorescent in situ hybridization. CI-inducing *w*Mel+ and CifAB-expressing males had 1.2- to 2.4-fold less AAGAG lncRNA relative to their aposymbiotic counterparts (Fig. 2 and fig. S3). Upon individual expression, CifA caused a 1.3-fold reduction in AAGAG lncRNA relative to CifB (Fig. 2, A and B). Thus, CifB does not interfere with CifA's ability to access spermatocyte RNA and cleave it in CI males. Notably, CifA harbors a bipartite nuclear localization signal (bNLS) essential for nuclear targeting, CI, and the H-P exchange (*13*). Mutant CifA with a deleted bNLS ($CifA_{\Delta bNLS}$) had significantly higher AAGAG RNA compared with CifA and CifAB lines (Fig. 2, A and B), corroborating the functional importance of CifA nuclear import in accessing CI targets.

To directly test the involvement of the lncRNA in CI, we used transgenic flies with RNA interference (RNAi)–mediated knockdown of the AAGAG lncRNA (*25*). If the lncRNA is causal to CI, then depleting the AAGAG lncRNA in the presence of *w*Mel should increase wild-type CI. We assessed CI with a standard embryonic viability assay by measuring the percentage of embryos that hatched into larvae. *w*Mel-carrying AAGAG-knockdown males (AAGAG_KD+) induced approximately threefold more CI (median embryonic hatching = 11.8%) upon mating with uninfected (*w*Mel–) females compared with control males (Scramble_KD+) with a randomized A and G content that induced intermediate levels of CI (median embryonic hatching = 35.6%) (Fig. 2C). These findings indicate causal interaction between *Wolbachia* and AAGAG lncRNA depletion on CI. Control AAGAG-knockdown males without *Wolbachia* (AAGAG_KD–) did not recapitulate CI on their own (fig. S4), indicating that AAGAG lncRNA depletion alone is not the sole cause of CI and must operate in conjunction with other CI modifications by the Cifs. Both CifA and CifB localize to spermatogonia and spermatocyte nuclei (*13*); thus, it is possible that Cifs act on AAGAG lncRNA and perhaps other spermatogenesis-related lncRNAs (*24*, *26*) earlier during premeiotic spermatogenesis to prime cells and/or chromosomes to affect downstream postmeiotic sperm chromatin organization. These findings are consistent with single-cell transcriptome sequencing in which *Wolbachia* alter fly gene expression in early stages of spermatogenesis, leading to downstream sperm defects (*27*). Altogether, the role of CifA in depleting AAGAG lncRNA suggests that CifA RNase activity is central to establishing the CI modification during early sperm development.

CifA and CifB enhance DNA damage in developing CI spermatids

DNA damage and repair are typical features facilitating the H-P exchange during the canoe stage of spermiogenesis to tightly pack the sperm chromatin (*28*). However, in animals, excessive DNA breaks result in abnormal chromatin integrity, reduced male fertility, and

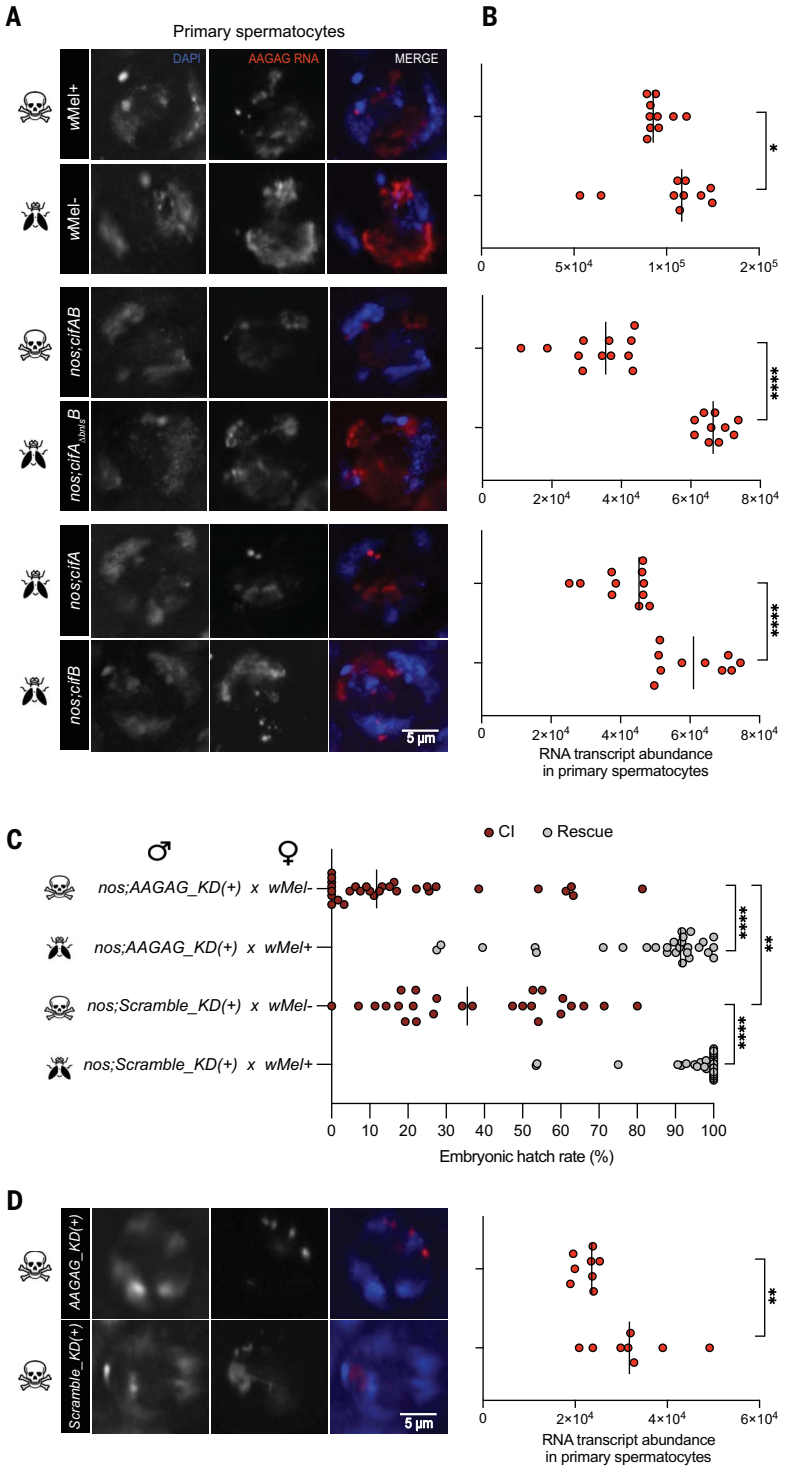

Fig. 2. CifA in situ RNase activity depletes AAGAG lncRNA in association with CI. Fluorescent in situ hybridization (FISH) assay was performed on testes (n = 15) squashes from <8-hours-old males to visualize and quantify the AAGAG repeat lncRNA abundance in primary spermatocytes (*25*). (**A**) Compared with the *w*Mel-negative and transgenic non-CI control line CifA$_{\Delta bnIs}$B, AAGAG lncRNA (red) is less abundant in primary spermatocytes, marked by 4′,6-diamidino-2-phenylindole (DAPI) staining (blue), of *w*Mel+ and dual-transgenic CifAB lines, respectively. CifA expression depletes lncRNA, whereas CifB does not. (**B**) lncRNA signal intensity per spermatocyte was quantified in ImageJ, as described in fig. S3, and graphed. The *y* axis corresponds to the genotype labels shown on the left side of (A). (**C**) Hatch rate assay confirmed that AAGAG_KD(+) symbiotic males with depleted lncRNA result in stronger CI than negative control Scramble_KD(+) males. Each dot represents the percentage of embryos that hatched from a single male and female pair. (**D**) Representative lncRNA-FISH and quantification data are shown for AAGAG_KD(+) and Scramble_KD(+) sibling males to those used in the panel 2C hatch rate assay. Vertical bars in (B), (C), and (D) represent the median. *P < 0.05; **P < 0.01; ****P < 0.0001; calculated by Mann-Whitney pairwise comparison test. The skull icon represents CI, and the fly icon represents no CI.

embryonic inviability (*29*, *30*), suggesting a link to CI. Because Cifs alter the abundance of histone and protamine nucleoproteins (*13*) and both Cifs catabolize DNA, we hypothesized that they promote spermatid DNA damage in elongating spermatids. We used terminal deoxynucleotidyl transferase–mediated deoxyuridine triphosphate nick end labeling (TUNEL) staining to evaluate DNA fragmentation in wild type and transgenic *D. melanogaster* testes. TUNEL signals persisted at higher levels in CI-inducing *w*Mel+ and *cifAB* late-canoe spermatids, as well as occasionally in needle spermatids, than in non-CI controls (Fig. 3, A and B, and fig. S5) with significantly higher numbers of damaged bundles (Fig. 3C), validating that *Wolbachia* and the Cif enzymes enhanced in situ DNA damage during the elongation process. Single CifA and CifB also promoted spermatid DNA damage relative to the transgenic negative control (Fig. 3), confirming their in vitro enzymatic independence to cleave DNA. Notably, their individual impacts on DNA damage, as measured by corrected total cell fluorescence (CTCF) of the TUNEL signal (CifA median CTCF = 233.12; CifB median CTCF = 364.06) was approximately

equivalent to the DNA damage induced by dual expression of CifA and CifB (median CTCF = 506.42), indicating their additive effect (Fig. 3B). Moreover, CifA and CifB mutants that failed to cause CI (*31*) did not nick spermatid DNA in situ (fig. S6), suggesting that spermatid DNA damage contributes to the CI phenotype. By costaining TUNEL with Cif antibodies, we found that at the early canoe stage, both CifA and CifB signals localized at the tips of spermatid heads with TUNEL-positive signals (fig. S7). At the needle stage, damaged spermatids showed that CifA localized toward the tail and that CifB in the sperm head remained undetectable owing to poor antibody penetration in highly condensed nuclei, as shown previously (*13*). Consequently, we propose that Cif presence in early spermatogonia, spermatocytes, onion spermatid nuclei, and early canoe stage (*13*) prime the spermatid DNA for damage detected in late elongating stages of spermiogenesis. Our results are also consistent with those of a previous study on elevated oxidative DNA damage in CI spermatocytes (*32*). Altogether, CI sperm suffers increased DNA damage beyond levels essential for a normal H-P transition and chromatin architecture.

CI embryos succumb to DNA damage

Because CifAB-expressing CI males suffer from depleted lncRNA and enhanced DNA damage, resulting in sperm development with altered H-P abundance, we next investigated whether fertilization by the compromised CI sperm causes adverse effects in embryos during nuclear divisions. Previous studies showed that *Drosophila* embryonic DNA damage is only evident in late stages of development ~6 hours after egg deposition (AED) toward gastrulation (*33*–*35*), as the cells at this stage become hyperprolifertive, and hence, more susceptible to damage (*36*–*38*). Although CI is often associated with a first–mitotic division defect within 1 hour of egg fertilization, additional developmental defects also occur in late CI embryos developing through the preblastoderm divisions, syncytial, and cellularized blastoderms (*10*, *39*–*41*). We collected embryos aged 0 to 1 hour, 1 to 2 hours, and 2 to 3 hours AED from CI, non-CI, and rescue crosses. We used the pH2Av marker, a variant of histone H2Av that is phospohorylated in response to DNA damage (*42*, *43*). In agreement with previous reports (*33*–*35*), we did not detect pH2Av signals indicative of DNA damage in early 0- to 1-hour-old CI embryos (*nos;cifAB* x *w*Mel–) arrested after the first mitotic division, as well as 0- to 1-hours-old and 1- to 2-hours-old rescue embryos (*nos; cifAB* x *w*Mel+) undergoing rounds of nuclear divisions (fig. S8) (*34*). However, we started detecting DNA damage signals in 2- to 3-hours-old AED CI embryos during cellular blastoderm formation (nuclear cycles 12 to 14) (*44*), when dividing nuclei migrate to the cortex periphery of the embryo (*34*, *44*). We observed

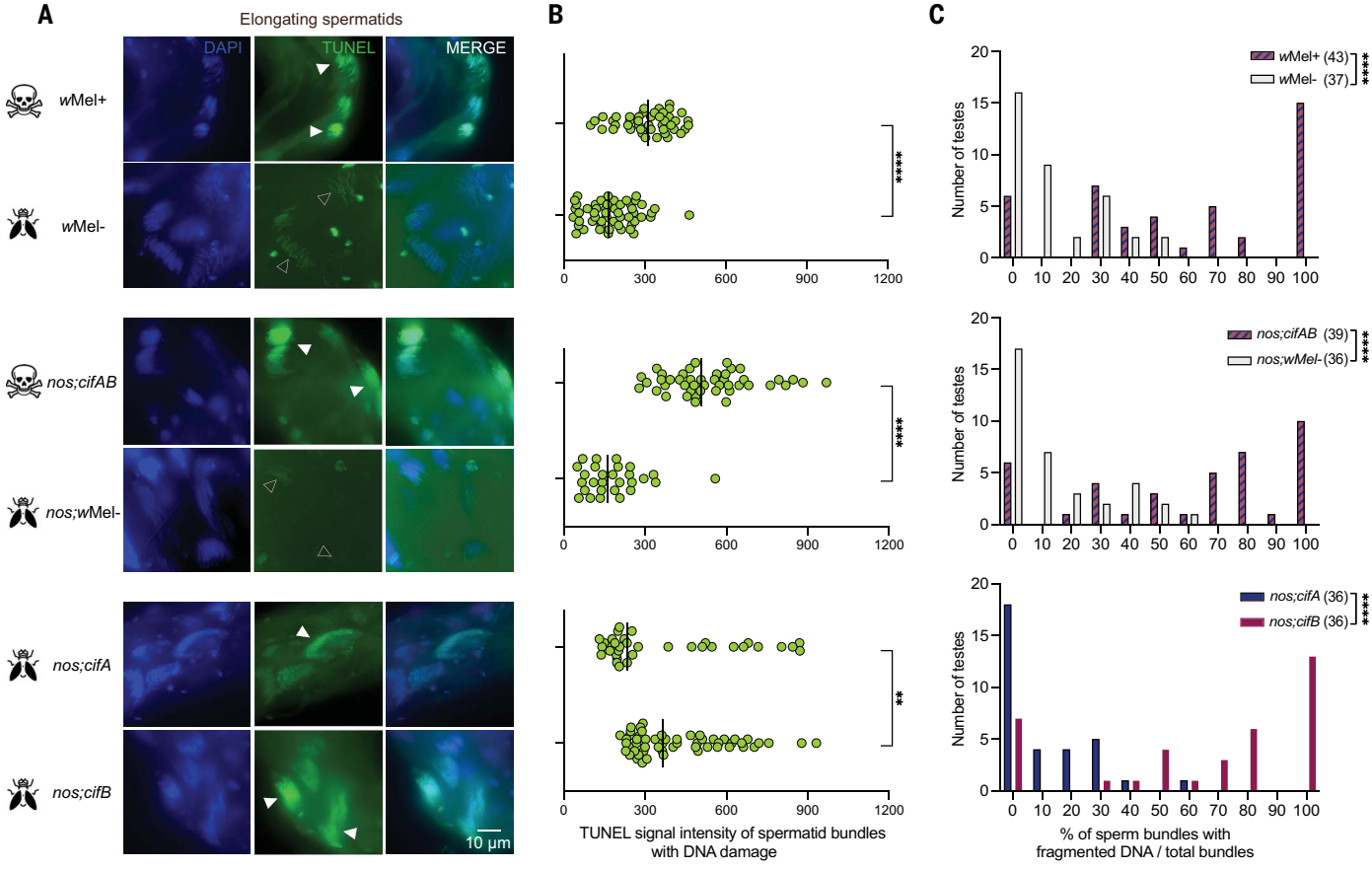

Fig. 3. CifAB in situ DNase activity enhances DNA damage in elongating spermatids. TUNEL staining on testes squashes from <8-hours-old males was performed to visualize and quantify sperm bundles with DNA breaks. (**A**) Representative images of spermatid bundles with DNA damage from each treatment group are shown. Images were taken using Keyence All-in-One confocal microscope at 100× magnification. Compared with the *w*Mel– control (empty arrowheads), DNA break signals marked by TUNEL (green) were highly intense in the wild-type *w*Mel+ and dual transgenic CifAB lines at the canoe stage of spermiogenesis (solid arrowheads). DAPI staining (blue) labels the spermatid nuclei. Upon individual expression, CifB induced higher DNA damage than CifA. (**B**) TUNEL signal intensity from spermatid bundles was quantified in ImageJ and graphed. Vertical bars represent the median. (**C**) Total sperm bundles and those with fragmented DNA were manually counted. The numbers of testes investigated are shown in parentheses next to the genotype. Uncropped images of testes from CI versus non-CI males with total damaged bundles with high versus low TUNEL intensity are shown in fig. S5. $^{**}P < 0.01$; $^{****}P < 0.0001$; calculated by Mann-Whitney pairwise comparison test.

intense pH2Av signals in dense chromatin nuclei with cellular shrinkage in 32% of total CI embryos that were in late developmental stages, suggesting that higher DNA damage associates with late embryonic defects and death (Fig. 4, A and D). In some embryos at the same stage, we observed chromatin-bridging defects colocalized with DNA damage signals and arrested chromatids at the metaphase as shown earlier (*41*) (Fig. 4, B). These embryos also included a portion of normally developed nuclei with no pH2Av signals (Fig. 4, B), indicative of a distinct effect with which CI associates throughout development. This DNA damage may precipitate the recent observation of nuclear fallout in the peripheral cells of CI embryos (*41*). We propose that late CI embryos (2 to 3 hours AED) that escape the first mitotic defect accumulate fatal damage through successive nuclear divisions, leading to mortality.

By contrast and as expected, rescue and non-CI embryos (*nos;cifA* x *w*Mel–, *nos;cifB* x *w*Mel–, and *nos;cifA*$_{\Delta bnls}$*B* x *w*Mel–) showed either no or significantly less pH2Av signals undergoing normal nuclear division and development (Fig. 4, C and D). Our data reinforce that DNA integrity, damage, and repair are key aspects of Cif-mediated CI and rescue. Indeed, treating aposymbiotic females with DNA repair chemicals suppressed CI (*45*). These results suggest that there is a CI cascade of damage, spanning prefertilization chromatin integrity changes to postfertilized embryos.

Mutagenesis links altered sperm development to embryonic DNA damage

We investigated whether the phenomena of lncRNA depletion and embryonic DNA damage are linked. We took advantage of two CifA mutant proteins previously characterized for the CI trait (*31*). CifA_3B contains amino acid substitutions that ablate CI and occur in a predicted domain of unknown function (DUF) that is distantly homologous to a Puf-family RNA-binding domain. CifA_4B contains substitutions that do not ablate CI and occur in a putative sterile-like transcription factor domain (STE) at the C-terminal of the protein (*31*), highlighting that different CifA domains or residues related to RNA processing possess distinctive molecular functions involved in CI.

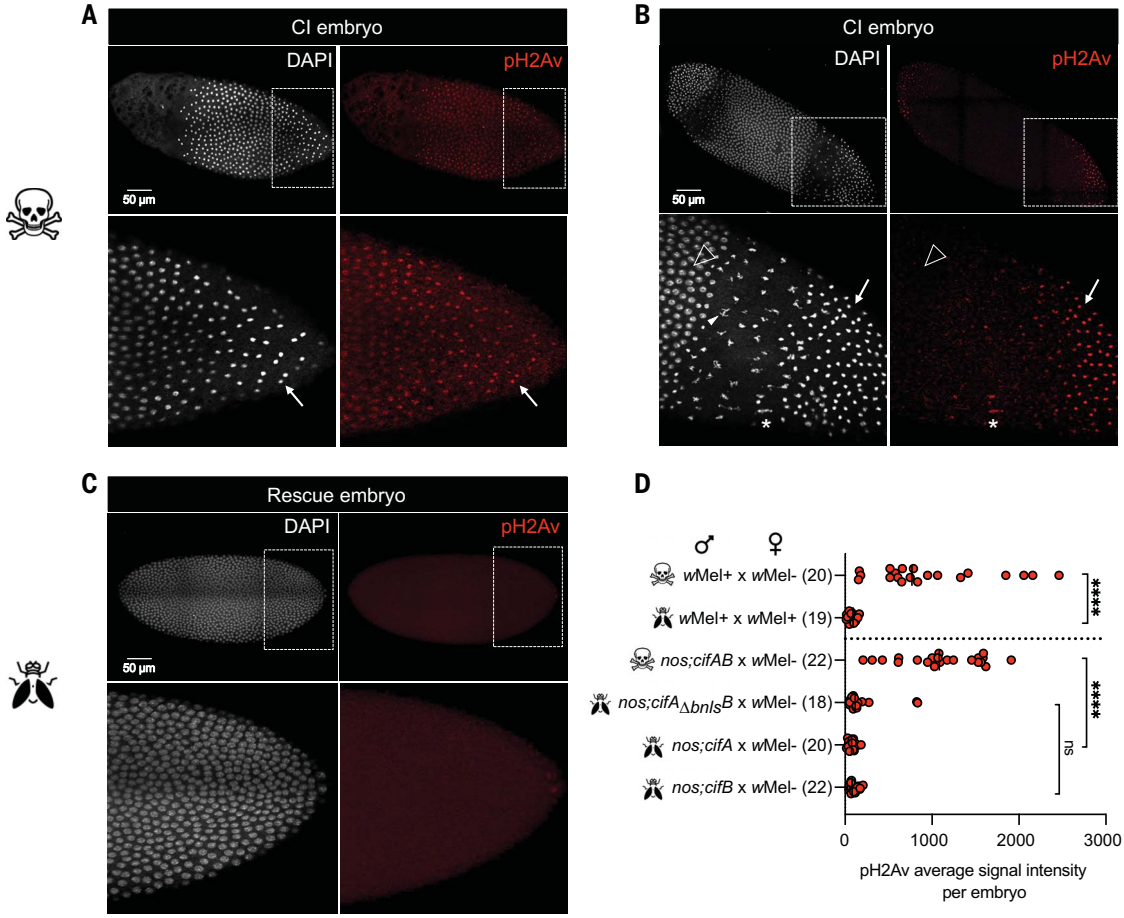

Fig. 4. Late-stage CI embryos suffer from DNA damage. (**A** to **C**) (Top) Representative images of 2- to 3-hours-old CI embryos (*w*Mel+ males × *w*Mel– females) during cellular blastoderm formation (nuclear cycles 12 to 14) exhibit intense pH2Av signals (red) indicative of DNA damage compared with that of rescue embryos (*w*Mel+ males × *w*Mel+ females). pH2Av is a histone H2Av variant that phospohorylates in response to DNA damage (*42*, *43*). (Bottom) Magnified images of boxed regions in (A), (B), and (C) top panels, respectively. (A) CI embryonic nuclei on polar ends undergo shrinkage and are distantly spaced with condensed chromatin (white arrows), likely becoming apoptotic leading to embryonic death. DAPI (gray) staining labels the embryonic nuclei. (B) In CI embryos, a CI-defining chromatin bridging is marked by an asterisk colocalized with DNA damage signal (red). In the same embryo, nuclei in the middle (empty arrowhead) developed normally with no pH2Av signals. A white solid arrowhead indicates a distinct missegregating chromosomal feature in the region between the middle and polar end of the embryo that contains condensed chromatin with DNA damage (white arrows). (C) A rescue embryo develops normally with evenly spaced embryonic nuclei lacking DNA damage. Full embryo confocal images were acquired with a Zeiss LSM880 confocal microscope at 63× magnification by using the tile-scan feature and automated stitching. (**D**) Data show the quantification of pH2Av signal intensity per embryo derived from CI and non-CI–rescue crosses. Values in parentheses correspond to the number of embryos scored. Vertical bars represent the median. A horizontal dotted line separates wild-type and transgenic cross types. ****P value < 0.0001; ns, not significant; calculated by Mann-Whitney pairwise comparison test.

The CI-ablating $CifA_3B$ mutant did not affect the AAGAG lncRNA in situ, whereas the CI-inducing $CifA_4B$ mutant reduced lncRNA abundance (Fig. 5A). We corroborated the correlation of depleted lncRNA with altered abundance of nucleoproteins in the developing sperm. $CifA_3B$ failed to recapitulate the CI-defining changes in histone and protamine abundance, whereas lncRNA-depleting and CI-causing $CifA_4B$ impaired histone removal in late-elongating spermatids and caused protamine deficiency in mature sperm (Fig. 5, C and D), as previously shown in CifAB-expressing CI males (*13*). We also connected the altered sperm architecture to CI-induced lethality by showing that CI-causing $CifA_4B$-fertilized embryos succumbed to DNA damage, whereas non–CI-causing $CifA_3B$ sperm did not cause embryonic DNA damage, and embryos developed normally (Fig. 5, B and E). The Cif-mutated residues are noncatalytic and partially buried at the structural level (*19*). Thus, it is plausible that these mutants may affect structural stability of the protein beyond the CI-related phenotypes we observed.

Altogether, transgenic expression of CI- and non–CI-causing CifA and CifB mutants in situ showed a genotype-phenotype association commencing prefertilization as lncRNA depletion in spermatocytes, enhanced DNA damage in elongating spermatids, and abnormal H-P abundance in maturing sperm. These errors correlated with postfertilization embryonic DNA damage associated with CI. Notably, the CI-causing $CifA_4B$ mutant links lncRNA depletion to CI, whereas the non-CI $CifA_3B$ mutant ablates lncRNA depletion and CI, thereby establishing CifA's RNase activity as important to the CI mechanism. Most CI-ablating CifB mutants also abolished spermatid DNA damage, specifying a correlation between CifB's DNase activity to CI. The lack of DNA damage in the CI-causing $CifA_4B$ mutant suggests that damage may either be under the detection limit or that it may be correlated but not incipiently causal to CI.

We summarize our findings in light of the host modification model of CI, in which modified sperm develop with compromised RNA and DNA content that precipitate a cascade of chromatin integrity changes, including fatal

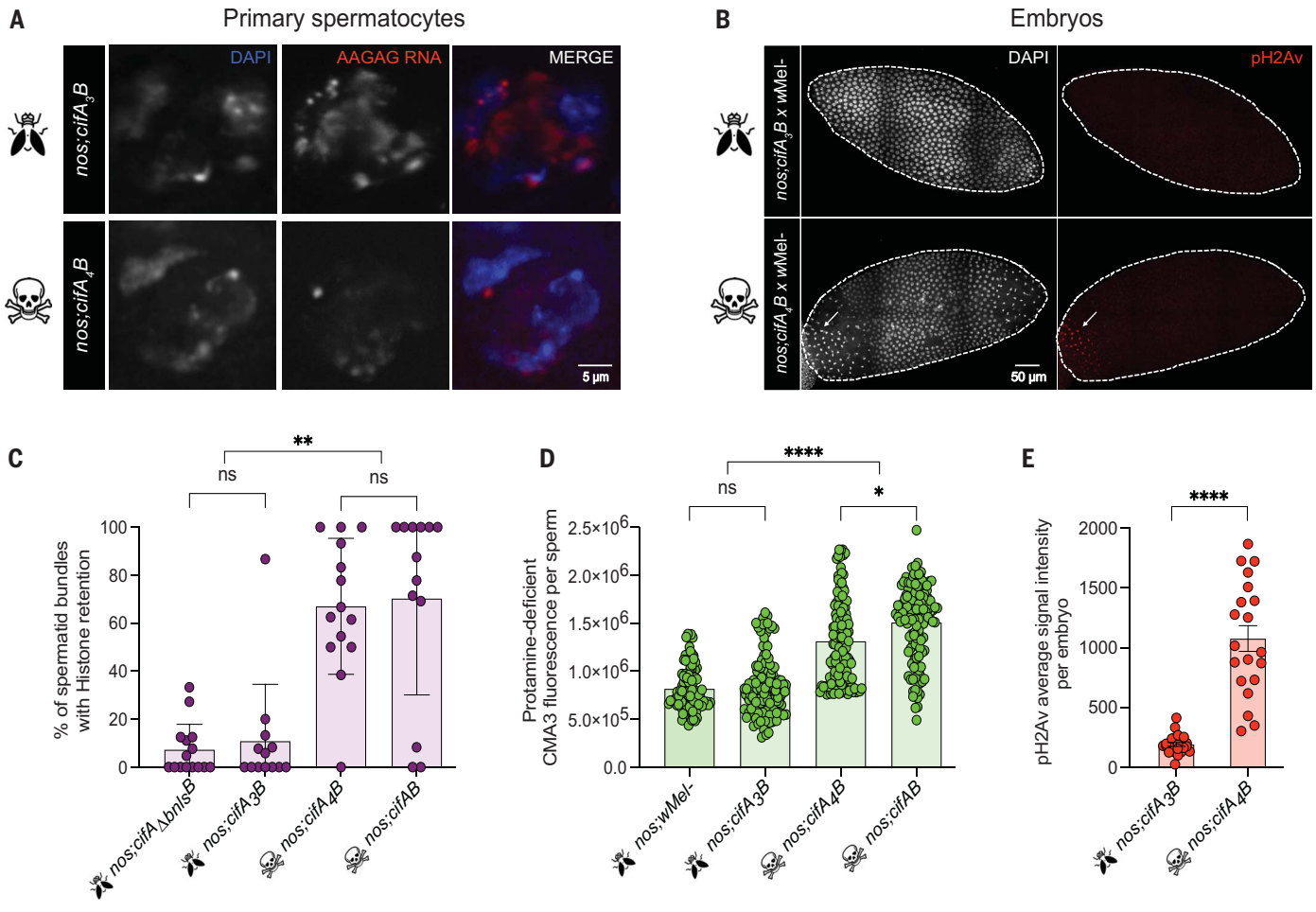

Fig. 5. CI induction and ablation directly link with AAGAG lncRNA depletion, impairment of histone-to-protamine transition, and DNA damage in embryos. (**A**) RNA-FISH on testes (n = 15) from <8-hour-old males of CI-inducing $CifA_4B$ and non-CI $CifA_3B$ mutant males (Fig. 2) showed that the $CifA_4B$ mutant depletes AAGAG lncRNA, whereas $CifA_3B$ does not. (**B**) CI embryos (*nos;cifA4B* males × *w*Mel− females) exhibited intense pH2Av signals (red) at the polar end (white arrow), which was indicative of DNA damage, compared with non-CI embryos (*nos;cifA3B* males × *w*Mel− females). Dotted periphery is drawn around the embryo shape. (**C**) CI and non-CI testes were immunostained to quantify histone-retaining spermatid bundles (purple) during late canoe stage of spermiogenesis (*13*). Non-CI lines ($CifA_3B$ and $CifA_{\Delta bnls}B$) showed significantly less spermatid bundles with retained histones compared with that of CI groups ($CifA_4B$ and CifAB). (**D**) Mature sperm from seminal vesicles were stained with fluorescent Chromomycin A3 (CMA3) stain (green) to detect protamine deficiency (*13*). CI sperm ($CifA_4B$ and CifAB) lack protamines compared with non-CI sperm ($CifA_3B$ and *nos*;*w*Mel−). (**E**) pH2Av signal intensity quantification per embryo derived from CI and non-CI crosses. Vertical bars represent mean, and error bars represent standard deviation. $^{**}P < 0.01$; $^{****}P < 0.0001$; ns, not significant; calculated by Mann-Whitney pairwise comparison test.

shifts in epigenetically regulated histone and protamine abundance (fig. S9). We hypothesize that postfertilization, the modified CI sperm with imbalanced protamine content experience chromatin remodeling defects, including delayed maternal histone deposition (*46*), replication stress, DNA damage, improper condensation, and delayed entry into first mitosis, succumbing embryos to a catastrophic death. We propose under the host modification model that CifA similarly mediates rescue of this paternal modification by altering maternal epigenetics and chromatin integrity during oogenesis in symbiotic females. By doing so, modified paternal and maternal chromatin synchronously enter the first mitosis in a fertilized embryo. Consistent with the mistiming model (*47*), the first mitosis now proceeds normally; consequently, there would be no further downstream DNA damage and replication defects in the embryo. The unmodified sperm from aposymbiotic *w*Mel– males will be compatible with embryos derived from either symbiotic or aposymbiotic females because maternal chromatin controls the entry timepoint into mitosis (*48*).

This study identifies prophage endonucleases modulating eukaryotic lncRNA and DNA that play crucial roles in animal reproduction. A cascade of early modifications established prefertilization in the testes ultimately results in postfertilization paternal-effect embryonic lethality. Notably, the effector Pne1 from the phage-like contractile injection system of the insecticidal *Photorhabdus* symbiont is also an endonuclease, and the translocated protein can kill insect cell lines (*49*). The discovery that intranuclear Cifs alter central-dogma features of sperm biology, spanning noncoding RNA depletion and DNA damage, reveals a molecular tangled bank of tripartie phage-endosymbiont-animal interactions that are vital to animal gametogenesis and embyrogenesis.

REFERENCES AND NOTES

1. J. J. Barr, *mSystems* **4**, e00105-19 (2019).
2. L. A. Weinert, E. V. Araujo-Jnr, M. Z. Ahmed, J. J. Welch, *Proc. Biol. Sci.* **282**, 20150249 (2015).
3. A. A. Hoffmann, M. Turelli, L. G. Harshman, *Genetics* **126**, 933–948 (1990).
4. R. M. Brucker, S. R. Bordenstein, *Trends Ecol. Evol.* **27**, 443–451 (2012).
5. B. Caputo *et al*., *Pest Manag. Sci.* **76**, 1324–1332 (2020).
6. X. Zheng *et al*., *Nature* **572**, 56–61 (2019).
7. W. A. Nazni *et al*., *Curr. Biol.* **29**, 4241–4248.e5 (2019).
8. C. Indriani *et al*., *SSRN* (2020); https://dx.doi.org/10.2139/ssrn.3544812.
9. J. D. Shropshire, B. Leigh, S. R. Bordenstein, *eLife* **9**, e61989 (2020).
10. D. P. LePage *et al*., *Nature* **543**, 243–247 (2017).
11. J. F. Beckmann, J. A. Ronau, M. Hochstrasser, *Nat. Microbiol.* **2**, 17007 (2017).
12. J. D. Shropshire, J. On, E. M. Layton, H. Zhou, S. R. Bordenstein, *Proc. Natl. Acad. Sci. U.S.A.* **115**, 4987–4991 (2018).
13. R. Kaur, B. A. Leigh, I. T. Ritchie, S. R. Bordenstein, *PLOS Biol.* **20**, e3001584 (2022).
14. T. Yu *et al*., *Science* **379**, 1358–1363 (2023).
15. I. A. Murray, S. K. Stickel, R. J. Roberts, *Nucleic Acids Res.* **38**, 8257–8268 (2010).
16. H. Chen, J. A. Ronau, J. F. Beckmann, M. Hochstrasser, *Proc. Natl. Acad. Sci. U.S.A.* **116**, 22314–22321 (2019).
17. G. Sun, M. Zhang, H. Chen, M. Hochstrasser, *mBio* **13**, e0317721 (2022).
18. A. R. I. Lindsey *et al*., *Genome Biol. Evol.* **10**, 434–451 (2018).
19. H. Wang *et al*., *Nat. Commun.* **13**, 1608 (2022).
20. M. R. Singleton, M. S. Dillingham, M. Gaudier, S. C. Kowalczykowski, D. B. Wigley, *Nature* **432**, 187–193 (2004).
21. E. Sisáková, L. K. Stanley, M. Weiserová, M. D. Szczelkun, *Nucleic Acids Res.* **36**, 3939–3949 (2008).
22. G. Cenci, S. Bonaccorsi, C. Pisano, F. Verni, M. Gatti, *J. Cell Sci.* **107**, 3521–3534 (1994).
23. C. Chu, K. Qu, F. L. Zhong, S. E. Artandi, H. Y. Chang, *Mol. Cell* **44**, 667–678 (2011).
24. K. Wen *et al*., *Genome Res.* **26**, 1233–1244 (2016).
25. W. K. Mills, Y. C. G. Lee, A. M. Kochendoerfer, E. M. Dunleavy, G. H. Karpen, *eLife* **8**, e48940 (2019).
26. V. Vedelek *et al*., *BMC Genomics* **19**, 697 (2018).
27. W. Dou, B. Sun, Y. Miao, D. Huang, J. Xiao, *Proc. Biol. Sci.* **290**, 20221963 (2023).
28. C. Rathke *et al*., *J. Cell Sci.* **120**, 1689–1700 (2007).
29. A. Agarwal, T. M. Said, *Hum. Reprod. Update* **9**, 331–345 (2003).
30. M. B. Hosen, M. R. Islam, F. Begum, Y. Kabir, M. Z. H. Howlader, *Iran. J. Reprod. Med.* **13**, 525–532 (2015).
31. J. D. Shropshire, M. Kalra, S. R. Bordenstein, *PLOS Pathog.* **16**, e1008794 (2020).
32. L. J. Brennan, J. A. Haukedal, J. C. Earle, B. Keddie, H. L. Harris, *Insect Mol. Biol.* **21**, 510–520 (2012).
33. E. Arama, H. Steller, *Nat. Protoc.* **1**, 1725–1731 (2006).
34. J. M. Abrams, K. White, L. I. Fessler, H. Steller, *Development* **117**, 29–43 (1993).
35. T. Harumoto, T. Fukatsu, B. Lemaitre, *Proc. Biol. Sci.* **285**, 20172167 (2018).
36. J. Bartek, *Mol. Oncol.* **5**, 303–307 (2011).
37. A. Baonza, S. Tur-Gracia, M. Pérez-Aguilera, C. Estella, *Front. Cell Dev. Biol.* **10**, 993257 (2022).
38. C. Zhang *et al*., *Oncogene* **34**, 2412–2412 (2015).
39. C. W. Lassy, T. L. Karr, *Mech. Dev.* **57**, 47–58 (1996).
40. G. Callaini, M. G. Riparbelli, R. Giordano, R. Dallai, *J. Invertebr. Pathol.* **67**, 55–64 (1996).
41. B. Warecki *et al*., *eLife* **11**, e81292 (2022).
42. T. Harumoto, H. Anbutsu, B. Lemaitre, T. Fukatsu, *Nat. Commun.* **7**, 12781 (2016).
43. J. I. Perlmutter *et al*., *PLOS Pathog.* **15**, e1007936 (2019).
44. S. Kotadia, J. Crest, U. Tram, B. Riggs, W. Sullivan, in *ELS* (Wiley, 2010).
45. A. Z. Momtaz *et al*., *Front. Microbiol.* **11**, 576844 (2020).
46. F. Landmann, G. A. Orsi, B. Loppin, W. Sullivan, *PLOS Pathog.* **5**, e1000343 (2009).
47. U. Tram, W. Sullivan, *Science* **296**, 1124–1126 (2002).
48. P. M. Ferree, W. Sullivan, *Genetics* **173**, 839–847 (2006).
49. I. Rocchi *et al*., *Cell Rep.* **28**, 295–301.e4 (2019).

ACKNOWLEDGMENTS

We thank three anonymous reviewers for their useful comments that improved the manuscript. We are grateful to G. Karpen (University of California, Berkley) for providing AAGAG and Scramble transgenic RNAi knockdown fly lines. We thank M. Grant for helping in hatch rate assays and E. Van Syoc for helpful discussions on CLEAN-based enzyme annotation analysis. We thank members of the Bordenstein lab, especially S. Bordenstein, L. Mendez, and L. Martinez, for helpful discussions during the writing process. We acknowledge Cell & Development Biology Equipment Resources at Vanderbilt University core facility for their help in using Odyssey CLx imaging system, the Proteomics Core of the Mass Spectrometry Research Center at Vanderbilt University for performing protein identification service, and the Huck Institute's microscopy core facility (RRID:SCR_024457) at the Pennsylvania State University for providing confocal imaging assistance. In the figures, the skull icon (representing CI) was taken from commons.wikimedia.org, and the fly icon (representing no CI) was from game-icons.net by Delapouite. **Funding:** This work was supported by National Institutes of Health awards R01 AI132581 and AI143725 to S.R.B, F32 AI140694 Ruth Kirschstein Postdoctoral Fellowship to B.A.L., National Science Foundation Graduate Research Fellowship DGE-144519 and National Science Foundation Postdoctoral Research Fellowship in Biology DBI-2010210 to J.D.S., and research funds from The Pennsylvania State University. The content is solely the responsibility of the authors and does not necessarily represent the official views of the funders. **Author contributions:** Conceptualization: R.K., J.D.S., B.L., and S.R.B.; Methodology: R.K., J.D.S., B.L., and S.R.B.; Investigation: R.K., A.M., and B.L.; Visualization: R.K.; Funding acquisition: J.D.S., B.L., and S.R.B.; Project administration: R.K. and S.R.B.; Supervision: R.K. and S.R.B.; Writing – original draft: R.K.; Writing – review and editing: R.K., A.M., J.D.S., B.L., and S.R.B.. **Competing interests:** S.R.B., R.K., and J.D.S. are authors on pending patent applications related to this work. The authors declare no other competing interests. **Data and materials availability:** All data are available in the main text and supplementary materials file.

SUPPLEMENTARY MATERIALS

science.org/doi/10.1126/science.adk9469
Materials and Methods
Supplementary Text
Figs. S1 to S11
Tables S1 to S4
References (*50*–*66*)
MDAR Reproducibility Checklist
Data S1 to S3
Raw Data

Submitted 19 September 2023; accepted 30 January 2024
10.1126/science.adk9469